J Mater Sci: Mater Med (2006) 17: 539–546
DOI 10.1007/s10856-006-8937-z

Hydrothermal synthesis and nanostructure of carbonated calcium hydroxyapatite

V. Jokanović · D. Izvonar · M. D. Dramićanin · B. Jokanović · V. Živojinović · D. Marković · B. Dačić

Received: 19 April 2005 / Accepted: 10 August 2005

Abstract The influence of precursor concentration, pressure, temperature and time of hydrothermal synthesis on the development of calcium hydroxyapatite structure has been analyzed. The obtained results show that it is possible to adjust the conditions of hydrothermal synthesis from solutions of relatively high concentrations to obtain calcium hydroxyapatite nanopowders of well-defined structure. The relationship between the synthesis and the lattice parameters, as well as the crystallite size and the microstructure of synthesized hydroxyapatite has been established. The synthesized powders are preferentially carbonated hydroxyapatite of the B type in the form of agglomerates that accommodate two-modal size pores of 1.5–10 and 50–200 nm. The structure of calcium hydroxyapatite particles consists of crystallites 8–22 nm in size, bound within prime particles, which size is between 10 and 63 nm, that in turn form bigger agglomerates 200 nm in size, which further cluster building up agglomerates 5–20 μm in size.

V. Jokanović (✉) · M. D. Dramićanin
Institute of Nuclear Sciences "Vinča", P.O. Box 522, 11001 Beograd, Serbia and Montenegro
e-mail: vukomanj@ptt.yu

D. Izvonar
Faculty of Contemporary Arts, Kralja Petra 6, 11000, Belgrade, Serbia and Montenegro

B. Jokanović
TU Clausthal, Institut fur Metallurgie, Department Termochemie und Mikrokinetik, Clausthal, Germany

V. Živojinović · D. Marković
Clinic of Preventive and Pediatric Dentistry, School of Dentistry, 11000, Belgrade, Serbia and Montenegro

B. Dačić
Department of Chemical Engineering, University Ockland, Ockland, New Zeland

1. Introduction

Calcium hydroxyapatite (CHA) is a superior biocompatible material because it contains Ca^{2+}, $P0_4{}^{3-}$ and OH^- ions; the ions that human tissue and bone have in relatively high percentage. In the form of very fine crystals, CHA accounts for approx. 58 per cent of bones in mammals. Together with biocompatibility and non-toxicity it demonstrates excellent osteoconductivity [1–10], and is widely used for bone reparation and orthopedic replacements, as well as for dental replacement and reparation [10–12]. Due to its biocompatibility and chemical reactivity to different biomaterials, CHA is a potential drug transmitter [1].

An interesting research approach is the synthesis of hydroxyapatite with higher chemical and biochemical activity at the interface with living tissues (proteins of living organisms), providing in that way better ties between them. Designing of a hydroxyapatite structure with such properties requires that specific attention is paid to the synthesis conditions [6, 8–12]. The designing methods for hydroxyapatite may greatly differ and comprise different synthesis techniques to produce different densities of particles and different porosities of compacts and coatings.

Electronic properties of hydroxyapatite are strongly related to its microstructure and bonding types and are sensitive to various factors such as: the applied method of synthesis, Ca/P ratio, non-stoichiometry of composition, defects in the crystal lattice, size of nanocrystals, reaction of the surface with the surrounding atmosphere, etc [11].

Hydroxyapatite crystallizes in the form of hexagonal crystal cell ($\boldsymbol{a} = \boldsymbol{b} = 9.432$ A, $\boldsymbol{c} = 6.881$Å). The arrangement of

phosphate ions in the crystal structure is such to provide the channel structure, in which calcium atoms are located within two different surroundings, Ca (I) and Ca (II). The Ca (I) one is parallel to the **c**-axes bounding nine oxygen atoms, i.e., 3 atoms in each of the positions O (1), O (2) and O (3). The Ca (II) surroundings contains one O (1), one O (2), four O (3) and one OH^- ion. Ca (II) has a larger atomic radius than Ca (I). The substitution of the carbonate group occurs either in the PO_4^{3-} position (for the B type of apatite), or in the OH^- position (for the A type of apatite) [13–27].

The presence of different impurities in CHA causes the formation of different structural defects. These defects can generate the secondary bonds between hydroxyapatite and various organic groups inside the living cells, which may affect the behavior of hydroxyapatite in bone replacements. Special effects are attributed to H^+ and PO_4^{2-} ions that can, depending on the environment, be found in the form of OH^-, HPO_4^{2-} or H_2O. They can initiate structural changes in hydroxyapatite, and hence its chemical activity [11, 26, 29].

Hydroxyapatite ceramic is used as a protective coating of dental implants, in the bulk form of low (type B) or high porosity (type F) for bone replacements, and in the granular form for the stuffing of bone defects [8–11]. Commonly released ions from hydroxyapatite ceramic are Ca^{2+} and PO_4^{3-} ions that are normally present in tissue fluids and therefore there is no allergic or immunology reaction of the tissue to it. In addition, mitigant characteristic of hydroxyapatite enables proliferation of patron-ageing living - cells at the hydroxyapatite ceramic/living tissue interface facilitating the creation of new bones through the process of osteogenesis [8–11].

Kinetics of chemical processes at the hydroxyapatite/living tissue interface is greatly affected by hydroxyapatite properties, mainly by its defectiveness and consequential surface activity [1, 21–27].

The investigation has been aimed to find out: (i) the relationship between the structure of hydroxyapatite (lattice parameters and disposition of constituent ions in the structure) and the parameters of hydrothermal synthesis, and (ii) specific characteristics of the hydroxyapatite microstructure. It is important because all the smallest synthesized – principle – particles are nanometer in size (the smallest particles identified by BET method). However, their average size and distribution may vary depending on the synthesis conditions.

2. Materials and methods

2.1. Processing of calcium hydroxyapatite

2.1.1. Powder synthesis

Shells of chicken eggs calcined at 900°C, till complete carbon removal and dissociation of $CaCO_3$ to CaO, and Merk's pro analysis quality $(NH_4)_2HPO_4$ were the precursors for CHA synthesis. Precursor solutions were prepared using a two-solution procedure:

i) 500 ml of 3.02 cmol solution of $Ca(OH)_2$ (solution 1) and 500 ml of 2.32 cmol of $(NH_4)_2HPO_4$ (solution 2).
ii) 500 ml of 7.55 cmol solution of $Ca(OH)_2$ (solution 1) and 500 ml of 5.7 cmol of $(NH_4)_2HPO_4$ (solution 2),
iii) 500 ml of 1.51 cmol solution of $Ca(OH)_2$ (solution 1) and 500 ml of 1.16 cmol of $(NH_4)_2HPO_4$ (solution 2),

The $(NH_4)_2HPO_4$ solutions were subsequently poured into $Ca(OH)_2$ solutions and vigorously mixed. Finally, 0.1 N HCl or $(NH_4)OH$ solution was added into the above given solutions to correct the pH value to 7.4.

The solution mixture content in a glass, covered with glass pane, was brought into an autoclave where it was autoclaved under predetermined conditions (temperature, pressure and time), given in Table 1. Notice that time needed for reaching the required temperature and pressure of the autoclaved solutions varied from 1 hr, for sample 4, to 1.5 hr, for sample 6. After that, the solutions were kept under these conditions for some time (2–8 hrs).

After hydrothermal treatment in the autoclave, precipitates were decanted from glasses, dried at 80°C for 48 hrs, disintegrated, washed with deionized water, and ultracentrifuged in order to get the purest possible CHA.

Table 1 Processing parameters of CHA synthesis

		Processing parameters		
Sample	Concentration	Temperature (°C)	Pressure (barr)	Time (h)
1	iii	150	5	8
2	ii	150	5	8
3	i	150	5	2
4	i	150	5	5
5	i	120	3	8
6	i	150	10	8
7	i	150	5	8
8	i	150	5	6.5
9	i	180	15	8

2.1.2. Powder characterization

An X-ray diffraction (XRD) method (Philips PW 1050) with Cu-Kα_{1-2} radiation was used for phase analysis of CHA and determination of crystallite size and lattice parameters. Data were analyzed in the range of 2θ from 9 to 67° with a scanning step of 5°, and exposition time of 2 sec per a step. The lattice parameter values were determined from the characteristic diffraction patterns using Reitveld's full profile method and the Koalarie computer software [30,31].

This program simultaneously gives data for hydroxyapatite crystallite sizes, based on Sherer's equation $d = K\lambda/B\cos\theta$, where d (in nm) is the average diameter of crystallites, K is the shape factor, B is the width of the (002) diffraction at the half of its maximum height, λ is the wave length of used X rays, and θ is the Brag diffraction angle.

A PERKIN ELMER 983G IR spectrometer, with KBr pastille, was used for CaHAp powder characterization. The analysis was made in the wave number range from 4000 to 400 cm^{-1}.

A scanning electron microscope (SEM JEOL 5300) was used to analyze the morphology, size distribution and the average size of CHA particles at the level of their largest agglomerates as well as their constituents – the smallest agglomerates of hydroxyapatite were 200 nm in size. Prior to SEM analysis, the as-prepared samples were suspended in ethanol and dispersed by ultrasound for 10 min and then the powder samples for the SEM analysis were coated with gold by the PVD process. The average particle size was calculated from the SEM micrographs with more than 100 particles.

An energy dispersive spectrometer (QX 2000 – Oxford Instruments) combined with SEM and multichannel analyzer was used to estimate the chemical homogeneity of synthesized CHA. The chemical homogeneity was assessed via Ca/P intensity ratio by using the ZAF (Link Company) software package, which compares the intensity of X-ray fluorescent emission from the surface of synthesized CHA with the standard sample.

The nitrogen gas absorption BET method (Sorptomatic 1990, Termoquest CE Instruments) was used for determination of the specific surface areas of CHA powders. The samples (0.20–0.22 g) for absorption measurement were thoroughly degassed at 150°C for 3 hrs.

Knowing absorbed volume of N_2 (purity 99.99%), specific surface areas of CHA powders were determined applying the BET method (based on correlation $p/(V_{ads}(p^0 - p))$ vs. p/p_0, where p_0 is the saturation pressure, p is the equilibrium pressure, V_{ads} is the absorbed volume of nitrogen). In addition, the Dubinin Radushkevich method (correlation $\log(V_{ads})$ vs. $\log^2(p^0/p)$ for determination of the specific surface area was used, too.

The volume of pores was evaluated using the Gurvich correlation V_{ads} vs. p/p^o. The average and the maximum radius of pores and the cumulative volume of all pores were determined using the Lecloux & Pirard method based on Dollimore Heal Pore-sizes standard absorption isotherm.

The assumption that the synthesized particles are spheroids enables the calculation of the average radius of particles ($d_{BET} = 6/\rho S_w$) where S_w is the specific surface area, and $\rho = 3.156$ g/cm^3 is the theoretical density of synthesized CHA powders.

3. Results and discussion

3.1. X-ray diffraction

A comparison of the values obtained for the lattice parameters of all synthesized hydroxyapatite samples with the theoretical ones shows that all values except those for the sample 5 are very close to the value for pure hydroxyapatite given as the standard. The found values for both lattice parameters are mostly slightly lower than those given in Table JCPDS No.9-423) [32].

The values of lattice parameters, evaluated by Reitveld's methods [30, 31], for various CHA samples, are only slightly different. Also, the differences in crystallite size and sharpness of some characteristic diffraction patterns can clearly be noticed.

Variation in precipitation parameters and amounts of the solid and the liquid phase, i.e., the quantity of apatite in the solution from which it precipitates, are given in Table 1. Temperature, pressure and time of the hydrothermal precipitation were analyzed separately to assess whether any of these parameters has particularly important influence on the crystal structure and size of the obtained crystallites, Table 2.

Although the change in crystal lattice parameters with varied solution concentrations is negligible, a trend of the change can be observed; the value of the cell parameter ***a*** increases and the value of the parameter ***c*** decreases to the extent not to be overlooked. However, the more apparent is the change in crystallite size with the change in apatite concentration, which varies from 12.5 nm, for the precipitate with the highest concentration of apatite (sample ii), to 18 nm for the precipitate with the lowest concentration of apatite (sample iii). The finest grain structure of CHA is a

Table 2 Crystal lattice parameters and crystallite size of CHA powders

	Sample								
a, c, cs	1	2	3	4	5	6	7	8	9
a, nm	0.9427	0.9430	0.9428	0.9429	0.9412	0.9429	0.9428	0.9428	0.9430
c, nm	0.6877	0.6874	0.6882	0.6878	0.6843	0.6874	0.6877	0.6878	0.6870
cs, nm	18	12.5	15	15	8	21	16.5	16	22

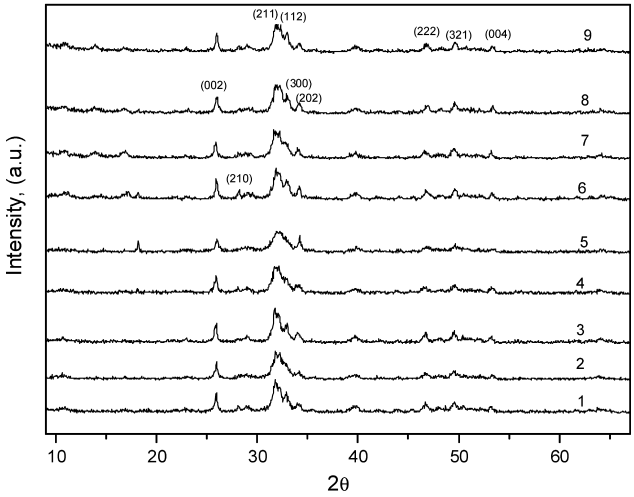

Fig. 1 X-ray diffraction of the CHA powders.

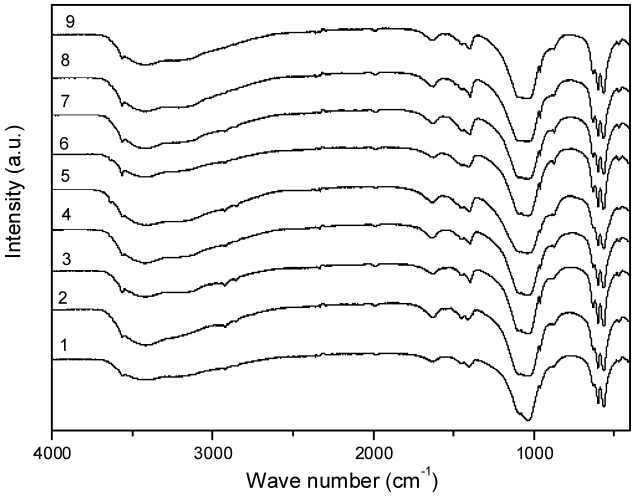

Fig. 2 IR spectra of the CHA powders.

result of increased number of crystallization centers during precipitation process.

The differences between the crystallite sizes are also observed for all other CHA samples obtained from medium and the highest concentration solutions (samples i and ii, respectively).

The X-ray diffractograms, Fig. 1, show that diffraction peaks for (002), (211) and (300) crystal facets of CHA are sharper for the samples precipitated from solutions with the lowest concentration of the solid phase than for CHA precipitated from those with medium or the highest concentration of the solid phase.

The increase in temperature and pressure of hydrothermal precipitation for the same time interval has similar effect on the lattice parameters of synthesized CHA, as the decrease in the solid phase concentration; i.e., the parameter **c** decreases while the parameter ***a*** increases with increasing temperature and pressure. Thus, the temperature and pressure increase has similar effect on the lattice parameters as the decrease in concentration of the solid phase at the beginning of hydrothermal treatment. Among synthesized samples, the sample precipitated at the lowest temperature (sample 5) has the lowest values of the parameter ***a***, and outstandingly small crystallite size (8 nm). This sample gave a small diffraction peak at $2\theta = 18.2^{\circ}$, which was not identified to belong to any of known phases, and also a distinct peak, assigned to the CHA facet (003), beneath which another diffraction peak belonging to an additional calcium phosphate phase, not identified in our investigation, might hide. Diffraction patterns from (002), (211), (112) and (300) facets for all samples excluding sample 5 (synthesized at the lowest temperature and pressure) are similar in shape. Also, the differences in crystallite size between these samples are small corresponding to the similar sharpness of the above given characteristic peaks.

It is observed, except for the sample 3, which was hydrothermally treated for only 2 hrs, that longer hydrothermal treatment of the precursor solution in the autoclave yields higher values of parameters ***c*** and ***a***. It has been found that the sample 3 has the smallest crystallite size (12.5 nm), and that a prolonged treatment in the autoclave from 5 hrs to 8 hrs increases the crystallite size for 1.5 nm only. The best differentiated diffraction patterns originate from (002), (210), (211), and (300) planes of the samples autoclaved for 8 hrs (the longest hydrothermal treatment), the shortest time required for the consolidation of the CHA structure.

3.2. IR spectroscopy

The comparison of vibration energies and band shapes for different samples from IR spectra that correspond to the stretching mode of OH^- vibration at 3540 cm^{-1} shows insignificant differences between the samples [33, 34]. However, it should be noted that this vibration for the samples 1, 6, 7 and 9 is shifted to 3568 cm^{-1}. For samples 2, 3, 4 and 8, this vibration is shifted to 3561 cm^{-1}, while for sample 5 there are doublets at 3568 and 3647 cm^{-1}, Fig. 2.

Although it is difficult to elucidate the cause of such an energy shift and shape change, two causes seem likely. It can be a partial replacement of OH^- ions with the ions of impurities, primarily with CO_3^{2-} ions, which may cause shifting of the vibration energy (i), or perhaps splitting of the OH^- vibration, depending on the total number of ions replaced in the positions, otherwise, occupied with OH^- ions (ii). This is in accordance with the earlier investigation, which encompassed IR spectroscopy and ^1H and ^{31}P NMR mass spectroscopy [11].

The cause for such a shifting and perhaps splitting of this OH^- vibration, as concluded, is the appearance of H^+ ion in its different structural combinations, a possible

explanation for our cases. Such combinations include H^+ ions as the constitutive elements of H_2O molecules with their own characteristic vibrations in the energy span of 3440—3430 cm^{-1}. These vibrations can be assigned to absorbed water on the surface of nanosized hydroxyapatite [11]. Beside and simultaneously with this vibration, another vibration may appear, which corresponds to the OH^- ions that build up the crystal structure of hydroxyapatite for which the vibration at 3565 cm^{-1} is characteristic. And, finally there is the stretching mode of OH^- at 3744 cm^{-1} (Table 3).

The types of configurations of OH^- ions in the crystal cell of CHA can, also, play an important role in the shifting of the mentioned vibrations. These configurations can be sorted into the following several most important types: (i) normal or stretched chain type, OH:OH:OH; (ii) tail-tail type, HO:OH:HO:OH; and (iii) the configuration in which an impurity ion group is in the central position establishing around itself a symmetrical distribution of OH^- ions of the OH:X:HO type, where X stands for the impurity ion group, most probably CO_3^{2-} in this study, which replaces two OH^- ions and, as a bigger ion, deforms the bonds in the chain of OH^- ions [34]. According to the obtained data, all hydrothermal precipitates of CHA, most likely, possess a structure in which OH^- ions are partially replaced with CO_3^{2-} ones. Probably due to dominant participation the hydrogen ion bonds in the lattice of hydroxyapatite, the obtained structure is not of the A type but of the B type predominantly, where a number of PO_4^{3-} ions are replaced with the CO_3^{2-} ones. It cannot, however, be overlooked that a certain number of CO_3^{2-} occupies the OH^- instead of PO_4^{3-} positions. Nonetheless, the PO_4^{3-} ion is the most probably a replacement for CO_3^{2-} ions[11, 34].

It is possible that under certain precipitation conditions such as temperature higher than 150°C, and pressure over 5 bars, the replacement of CO_3^{2-} at the position B is dominant. While for higher concentration, lower temperature, and shorter time of hydrothermal synthesis, the number of CO_3^{2-} ions substituting the OH^- ones in their positions is a bit larger, characterizing the A type of carbonated hydroxyapatite.

The bending mode of the OH^- vibration, which appears at 1635 cm^{-1}, does not shift with the change in precipitation parameters. This band is observed in the 1628–1636 cm^{-1} range (at 1628 cm^{-1} for samples 6,7 and 8, and at 1636 cm^{-1} for other samples) [33, 34]. The bands, which characterize the stretching mode of the CO_3^{2-} vibrations that appear as doublets, with more or less obvious peaks for all samples were registered within the interval of 1400–1450 cm^{-1}, implying that carbonated hydroxyapatite was synthesized under all precipitation conditions. The asymmetric PO_4^{3-} stretching mode ν_3 detected for different precipitation conditions in slightly shifted bands appears at 1101–1022 cm^{-1} (samples 1 and 5), 1115–1008 cm^{-1} (sample 2), 1108–1022 cm^{-1} (sample 3), 1108–1015 cm^{-1} (sample 4), 1101–1008 cm^{-1} (sample 6), 1101–1015 cm^{-1} (samples 7 and 8), and at 1049–1022 cm^{-1} (sample 9).

These small differences in vibration bands, manifested in almost plated-out minimums, correspond to the asymmetric stretching mode of the PO_4^{3-} vibration. The narrowed plateaus can be ascribed to higher temperatures and pressures of precipitation, but this explanation should be taken with caution. However, it is likely that the most influential effect on such a negligible shifting of vibrations and changes in plateau widths originate from CO_3^{2-} ions that partially substituted PO_4^{3-} ions. Due to smaller size of the CO_3^{2-} ion compared with the PO_4^{3-} one, carbonated hydroxyapatite allows shifting of their vibrations towards higher wave numbers, broadening, in that way, the vibration bands for carbonated hydroxyapatite more than those for pure hydroxyapatite. The vibration at 872 cm^{-1} is one of the stretching modes and belongs to CO_3^{2-} ions. The band at 958 cm^{-1} identified as the ν_1 symmetric stretching mode of the PO_4^{3-} vibration is very weak for some samples and a bit stronger for others like sample 5. The band at 558–565 cm^{-1} and another at 473–485 cm^{-1} belong to the ν_2 symmetric starching mode of the PO_4^{3-} vibration [34].

The band registered at 630 cm^{-1} belongs to the liberation mode of the OH^- vibration. For all synthesized samples of CaHAp this band appears at the same wave number – there is no shifting – which would be expected if the replacement of OH^- with CO_3^{2-} ions, or any other impurity, had happened[11]. It is obvious that the B type of carbonated hydroxyapatite was obtained under all conditions of hydrothermal synthesis, and that the replacements at the positions of OH^- ions, revealed by changes in shape and position of the band at 3658 cm^{-1}, indicate that these changes are not caused predominantly by the substitution of OH^- by CO_3^2.

3.3. Microstructure characteristics of powder

Analysis of the SEM micrographs presented in Fig. 3 shows great similarities between the shapes and sizes of particles of all precipitated powders.

All powder samples, Fig. 3a–d, consist of agglomerates, which shapes are almost the same. And, always, the size of agglomerates is between 5 and 20 μm, and they were built up from fine particles 200 nm in size. The forms of agglomerates are irregular with oval edges due to spherical shapes of individual particles. The agglomerates as big as 40 μm can be found, the dominant ones, however, are those 10–20 μm in size. The fraction of agglomerates 5–10 μm in size is important, too.

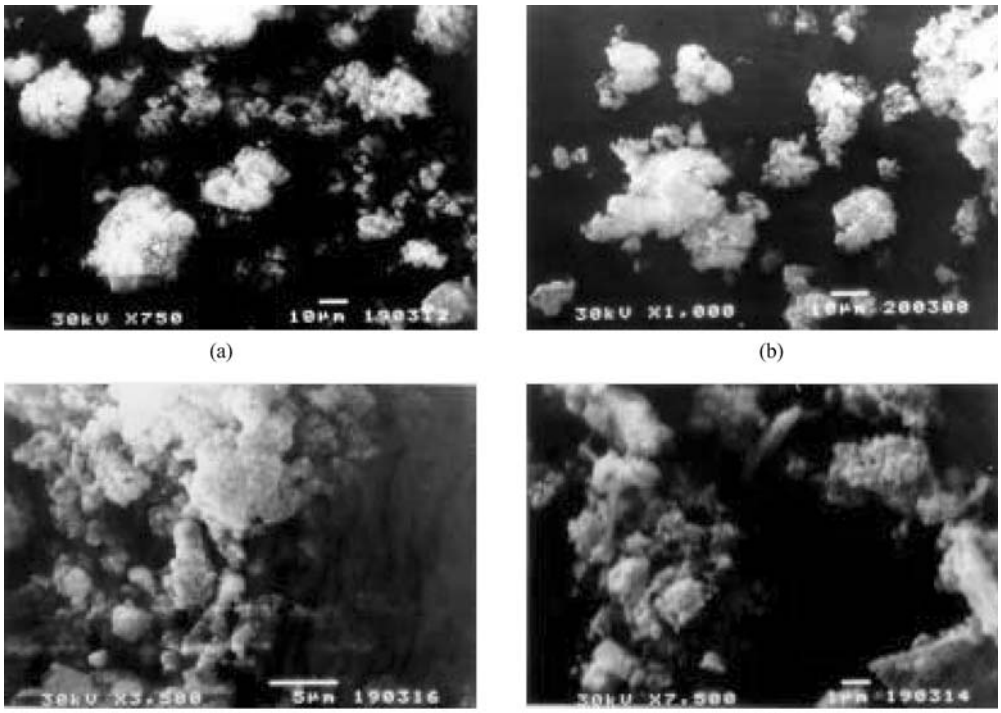

Fig. 3 Characteristic microstructures of precipitated hydroxyapatite; *a* (sample 5); *b* (sample 9); *c* and *d* (sample 7).

The size and shape of agglomerates and particles that form them are similar for all samples. Taking the value for crystallite size obtained by X-ray diffraction analysis to be a more precise one, it is evident that the microstructure of hydrothermally synthesized hydroxyapatite was developed through several stages, starting from crystallite structure of particles of 8–22 nm to fine sub-agglomerate particles up to 200 nm, which further cluster to give agglomerates 5–20 μm in size.

3.4. Specific surface area

The smallest particle size calculated from the value of the specific surface area, measured by BET absorption method, is about 30 nm. This value was obtained for sample 7 synthesized for 8 hrs at a temperature of 150°C and pressure of 5 bars. The particle sizes obtained from specific surface areas values are always larger than the crystallite sizes obtained by X-ray diffraction. By comparing these two values (particle size and crystallite size given in Tables 2 and 4), it seems plausible that the crystallites are the finest substructure elements of hydroxyapatite particles.

The difference between the crystallite size obtained by X-ray diffraction and the average particle size obtained by evaluation of the powder specific surface areas can be explained in two different ways. Firstly, this difference can be a result of the high extent of amorphousness of hydroxyapatite samples that consist of islands of nanocrystallites. The amorphous part of hydroxyapatite could be either on the surface or in the core of a particle, depending on the preferred crystallization mechanism of hydroxyapatite.

Otherwise, it is more probable that the primary particles were built up from a structured block mosaic, with well-defined small angle boundaries that make detection of these small crystallites as prime units of the hydroxyapatite

Table 3 Vibration frequencies of the nano-precipitated CHA

Assignation	Wave number (cm^{-1})
PO_4^{3-} band ν_2	471
PO_4^{3-} band ν_4	566
PO_4^{3-} band ν_4	574
PO_4^{3-} band ν_4	604
Structural OH	635
CO_3^{2-} group	873
PO_4^{3-} band ν_1	961
PO_4^{3-} band ν_3	1031
PO_4^{3-} band ν_3	1096
CO_3^{2-} group ν_3	1420
CO_3^{2-}grupa ν_3	1480
H_2O adsorbed ν_2	1645
Soluble CO_2 ν_3	2331
Soluble CO_2 ν_3	2360
H_2O adsorbed	3430–3440
Structural OH	3565–3568
OH stretching	3744

Table 4 Characteristic geometric parameters of hydroxyapatite powders obtained by analysis of nitrogen absorption isotherms

Number sample	1	2	3	4	5	6	7	8	9
Specific surface, m^2/g	48	110	75	77	180	32	62	65	30
$D_{BET(Č)}$, nm	40	17	23	24	10	59	31	29	63
D pore, nm	17	7	10	10	4	25	13	12	27
V pore, cm^3/g	0.232	0.099	0.132	0.139	0.058	0.342	0.180	0.168	0.365

microstructure impossible. In that case, both the size of these crystallites and the size of primary particles depend upon the conditions of the hydrothermal precipitation, as it can be seen in Tables 2 and 4.

Exceptionally high value of the specific surface area for sample 5 confirms that the true size of the primary hydroxyapatite crystallite unit, constituting an agglomerate particle, is approximately 10 nm, which is a bit higher than the value obtained by X-ray diffraction analysis. Therefore, it can be concluded that the primary constitutive units of sample 5 particles are crystallites. Based on sizes of primary particles obtained by X-ray diffraction, specific surface areas (BET method), and their comparison with the results of SEM microstructure analysis, it is clear that the CHA particles are clusters of small agglomerated particles approx 200 nm in size, filled up with considerably smaller primary particles ranging from 10 to 63 nm, which were built up from crystallites 8 to 22 nm in size. In addition, it is evident that the average pore size of CHA particles is 4–27 nm in diameter lining up well with the size of primary particles – agglomerate particles. The similar compliance was found for the pore volume per unit mass. The larger the particles the greater the average pore diameter and the total volume of pores.

The pore distribution is multimodal and follows up not only the size of primary particles – the smallest ones – but also the size of other particles packed into clustered powder particles. The pores are distributed from the smallest ones, in the range of 1.5–10 nm, up to the largest in the range of 50–200 nm. The largest pores correspond to the largest particles approximately 200 nm in size, clustered mostly into agglomerated particles 20 μm big, which can be seen in SEM micrographs of synthesized CHA.

4. Conclusion

The influences of precursor concentration, pressure, temperature and time of hydrothermal synthesis on the composition and microstructure of carbonated type of calcium hydroxyapatite have been investigated in this paper.

The results of X-ray diffraction analysis indicate the relationship between the synthesis conditions and the lattice parameters and crystallite size of CHA.

The IR spectroscopy results have shown that synthesized hydroxyapatite is preferentially of the B type and that the splitting of the vibration at 3568 cm^{-1} is primarily related to the changes in structure caused by H^+ ion.

Microstructure and specific surface area obtained by SEM and BET, respectively, clarify that all synthesized powders consist of agglomerated particles of 5–20 μm, built up from particles of approx 200 nm, and they are clusters of much smaller particles 10–63 nm in size. These smallest—primary—particles are built up from crystallites as big as 8–22 nm.

Acknowledgement We wish to acknowledge the support of the Ministry of Science and Environmental Protection of the Republic of Serbia. We also thank Drs M. MitriĆ and Z. NediĆ for their support related to XRD and IR analysis.

References

1. L. L. HENCH, *J. Amer. Ceram. Soc.* **74** (1991) 1487.
2. L. L. HENCH, *J. Amer. Ceram. Soc.* **81** (1998) 1705.
3. R. Z. LE GEROS and J. P. LEGEROS, Dense hydroxiapatite, in An Introduction to Bioceramics, *Adv. Ser. Ceram. 1,* edited by L. L. Hench and J. Wilson (World Scientific Publishing Co. Pte. Ltd., London, Hong Kong, Singapure, 1998) p. 139.
4. A. L. BOSKEY and A. S. POSNER, *J. Phys. Chem.* **80** (1976) 41.
5. E. D. EANES, *Calcit. Tiss. Res.* **5** (1970) 133.
6. S. ZHANG and K. E. GONSALVES, *J. Mater. Sci.: Mater. Med.* **8** (1998) 25.
7. L. L. HENCH, *Ceram. Bull.* **77** (1998) 67.
8. J. L. KATZ and R. A. HARPER, Calcium Phosphates and Apatites, in Enciclopedia of Materials Sciences and Engineering, edited by M. B. Bever (Pregamon Press, Oxford, 1986) p. 475.
9. G. HIENERAUER, T. MCGEE and R. KUDEJ, *Ceram. Bull.* **70** (1991) 1010.
10. G. ZAMBONIN and M. GRANO, Human Ostoblast. *Biomaterials* **16** (1995) 397.
11. R. N. PANDA, H. F. HSIEH, R. J. CHUNG and T. S. CHIN, *J. Phys. Chem. Solids.* **64** (2003) 193.
12. V. JOKANOVIĆ and D. USKOKOVIĆ, *Mater Trans. JIM* (2005) (in press).
13. E. G. NORDSTROM and K. H. KARLSSON, *J. Mater. Sci.: Mater. Med.* **1** (1990) 182.
14. T. KIJUMA and M. TSUTSUMI, *J. Amer. Ceram. Soc.* **62** (1979) 455.
15. I. NIKČEVIĆ, V. JOKANOVIĆ, M. MITRIĆ, Z. NEDIĆ, D. MAKOVEC and D. USKOKOVIĆ, *J. Sol. St. Chem.* **177** (2004) 2565.

16. V. JOKANOVIĆ, I. NIKČEVIĆ, B. DAČIĆ and D. USKOKOVIĆ, *J. Ceram. Proc. Res.* **5** (2004) 157.
17. W. EYSEL and D. M. ROY, *J. Cryst. Growth* **20** (1973) 245.
18. S. R. KIM, J. H. LEE, Y. T. KIM, D. H. RIU, S. J. JUNG, Y. J. LEE, S. C. CHUNG and Y. H. KIM, *Biomaterials* **24** (2003) 1389.
19. K. C. B. YEONG, J. WANG and S. C. NG, *Biomaterials* **22** (2001) 2705.
20. R. SANG-HOON, *Biomaterials* **23** (2002) 1147.
21. W. KIM, Q. YHANG and F. SAITO, *J. Mater. Sci.* **35** (2000) 5401.
22. B. DONAZZON, G. DECHAMBRE and J. L. LACOUT, *Ann. Chem. Sci. Mater.* **23** (1998) 53.
23. S. JINAWATH, D. PONGKAO, W. SUCHANEK and M. YOSHIMURA, *Int. J. Inorg. Mater.* **3** (2001) 997.
24. H. S. LIU, T. S. CHIN, S. Y. CHIU, K. H. CHUNG, C. S. CHANG and M. T. LUI, *Ceram. Int.* **23** (1997) 19.
25. M. AND RES-VERGES, C. FERNAND EZ-GONZALEZ and M. M. MARTINEZ-GALLEGO, *J. Europ. Ceram. Soc.* **18** (1998) 1245.
26. W. L. SUCHANEK, P. SHUK, K. BYRAPPA, R. E. RIMAN, K. S. TENHUISEN and V. F. JANAS, *Biomaterials* **23** (2002) 699.
27. K. CHENG, W. WENG, G. HAN, P. DU, G. SHEN, J. YANG and J. M. F. FERREIRA, *Mater. Chem. Phys.* **78** (2003) 767.
28. K. NAKAMOTO, Infrared and Raman Spectra and Coordination Compounds (John Wiley and Sons, New York, Chichester, Brisbane, Toronto, 1978).
29. G. PENEL, G. LEROY, C. REY, B. SOMBERT, J. P. HUVENNE and E. BRES, *J. Mater. Sci.: Mater. Med.* **8** (1997) 271.
30. H. RIETVELD, *J. App. Cryst.* **2** (1969) 65.
31. R. W. CHEARY and A. A. COELHO, *J. App. Cryst.* **25** (1992) 109.
32. JCPDS File No. 9-432, (CHA), International Center for Diffraction Data.
33. R. A. NYQUIST and R. O. KAGEL, Infrared Spectra of Inorganic Compounds, (3800-45 cm^{-1}), (Academic Press, New York and London, 1971) p. 493.
34. F. FRIEDEMANN and R. M. KNOBEL, *J. C. S. Dalton* (1977) 1136.